# Gaseous Jet in Supersonic Crossflow

S. D. Heister* and A. R. Karagozian†
*University of California, Los Angeles, California*

**This paper describes an analytical/numerical model representing the deflection and mixing of a single gaseous jet in supersonic crossflow. The jet cross section is modeled in terms of a compressible vortex pair that results from viscous and impulsive forces acting at the periphery of the jet. The behavior of the vortex pair is then combined with mass and momentum balances along the axis of the jet to form a model that describes the trajectory and mixing of the injected fluid. Due to complications associated with a supersonic crossflow, a numerical technique is used to solve for the inviscid outer flow and the position of the bow shock that envelopes the jet. This solution, combined with the computed flowfield of the compressible vortex pair associated with the jet, allows prediction of trajectories of these types of gaseous jets. Although there are limited experimental data for comparison with computed results, the present model is able to predict overall jet penetration (for perfectly or slightly underexpanded jets) to within 10% while requiring only a few seconds of computer time.**

## Nomenclature

$B$ = constant used in defining jet cross-sectional area
$C_D$ = Drag coefficient associated with elliptical cross section
$d$ = jet orifice diameter
$D_{bs}$ = bow shock standoff distance
$F_y$ = dimensionless force tending to separate vortices due to compressibility associated with vortex pair
$F_{yp}$ = dimensionless force tending to separate vortices due to jet underexpansion
$h$ = dimensionless vortex pair half-spacing
$k$ = recirculation cell perimeter-to-area ratio
$M$ = Mach number
$p$ = dimensionless pressure
$R$ = jet-to-crossflow momentum flux ratio $\equiv \rho_{jo}U_{jo}^2$
$s$ = dimensionless distance measured along jet trajectory
$t$ = dimensionless time
$U$ = dimensionless velocity
$w$ = dimensionless mass per unit depth within jet cross section
$x_o$ = dimensionless $x$-intercept of stagnation streamline
$X$ = streamwise coordinate of jet trajectory
$y_o$ = dimensionless $y$-intercept of stagnation streamline
$Z$ = transverse coordinate of jet trajectory
$\gamma$ = ratio of specific heats
$\Gamma$ = dimensionless vortex strength
$\rho$ = dimensionless density
$\phi_v$ = jet orientation angle

*Subscripts*
$\infty$ = freestream conditions
$j$ = local jet conditions
$jo$ = jet conditions at orifice
$c$ = recirculation cell condition

*Superscripts*
(-) = dimensional quantity

## Introduction

THE transverse jet in supersonic crossflow constitutes a very important problem in fluid mechanics that has several applications of practical importance, among them, fuel jet injection in scramjet combustors and thrust vector control for aerospace vehicles. Most of the early modeling efforts addressing this problem have been aimed at thrust vector control (TVC) applications of the transverse jet.[1-5] In this case, researchers are most interested in determining the total jet penetration depth and the resulting wall pressure distribution. The main applications are for supersonic crossflows, because TVC systems normally operate downstream of the throat in a DeLaval nozzle.

Figure 1 outlines some of the important features associated with a perfectly expanded transverse jet in a supersonic crossflow. The wall boundary layer typically separates two to three jet diameters ahead of the orifice by means of a separation shock. This shock then merges with a strong bow shock that envelopes the periphery of the jet. A boundary-layer reattachment shock is also present downstream of the injection point.

The jet cross section is observed to be "kidney shaped" for a jet injected transversely in either subsonic or supersonic crossflow.[6-8] This shape is developed due to the pressure field and viscous forces acting at the periphery of the jet. Observations by these and other researchers indicate the presence of a vortex pair structure that dominates the downstream cross section of the jet. If the jet is highly underexpanded, a normal shock or "Mach disk" will be present within the jet at a location within a few jet diameters of the orifice. The Mach disk becomes more important as the jet injection-to-crossflow pressure ratio increases.

Many of the modeling efforts for gaseous jets in supersonic crossflows have been aimed at developing semiempirical correlations using experimental data. Spaid and Zukoski[1] note that the bow shock generated by a jet in supersonic crossflow looks similar to that for a blunt nosed solid body, and they use this notion to correlate jet penetration depth with known injection and crossflow parameters by developing a force balance on an imaginary solid body. Other researchers[3-5] liken the shape of the bow shock to the upper half of an unsteady shock wave

Received Oct. 31, 1988; revision received April 24, 1989; presented as Paper 89-2547 at the AIAA/ASME/SAE/ASEE 25th Joint Propulsion Conference, Monterey, CA, July 10-12, 1989. Copyright © 1989 by A. Karagozian. Published by the American Institute of Aeronautics and Astronautics, Inc. with permission.

*Graduate Research Assistant, Mechanical, Aerospace, and Nuclear Engineering Department; presently Section Head, The Aerospace Corporation.

†Associate Professor, Mechanical, Aerospace, and Nuclear Engineering Departments. Member AIAA.

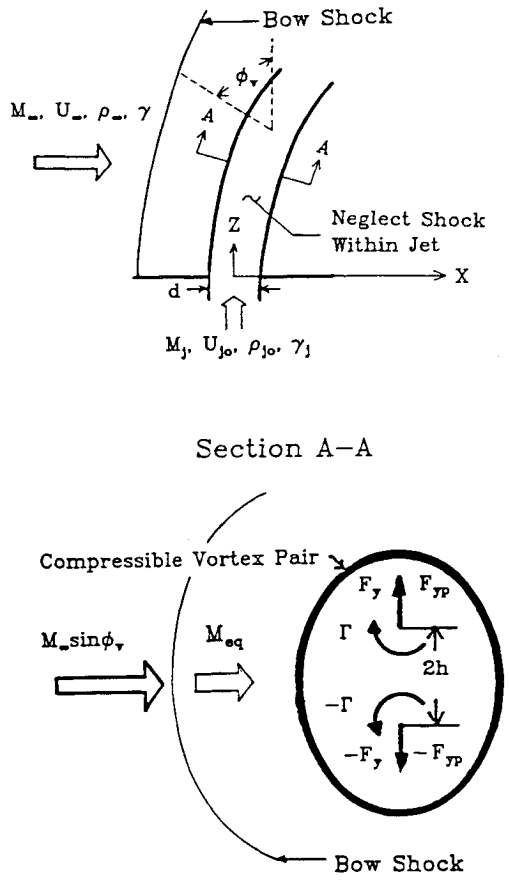


**Fig. 1 Schematic description of a gaseous jet in a supersonic crossflow, including a model of the jet cross section.**

resulting from the detonation of a cylindrical line charge, an analogy that predicts bow shock location fairly accurately.

All of these approaches ignore the structure of the transverse jet itself and contain implicit assumptions that the jet momentum remains constant, that no mixing occurs during turning, and that the injected flow turns sharply and then follows the injection surface. In addition, none of these approaches accounts for the Mach disk that can be present within the underexpanded jet. Schetz et al.[9] attempt to address the Mach disk problem with a series of experiments involving highly underexpanded sonic jets in supersonic crossflows. Introduction of an "equivalent back pressure" permits calculation of Mach disk location, and it is assumed that negligible jet penetration occurs after the Mach disk.

Billing and coworkers[10, 11] contribute the first model which considers jet spreading and momentum loss. The model is two-dimensional and predicts the jet trajectory by considering drag and centripetal forces acting perpendicular to the trajectory of the jet. The drag on the jet cross section is assumed to be equal to that of a 2-D circular cylinder with equivalent cross-sectional area, and is obtained from curve fits of experimental data for cylinders. Jet cross-sectional area as a function of distance along the jet is also obtained from curve fits of experimental data. This model, in additional to experimental work, [1, 2, 8] demonstrates that perfectly expanded jets can obtain better penetration than highly underexpanded jets because underexpanded jets lose much of their momentum in passing through the Mach disk.

To summarize, we note that these models for transverse jets in supersonic crossflow all suffer the following deficiencies: 1) a detailed pressure field about the cross-section of the jet is not provided, 2) no mixing of the jet and crossflow is allowed during jet turning, 3) effective back pressure values are estimated and are not calculated due to lack of pressure information around the jet, 4) jet spreading has never been predicted analytically, and 5) the jet cross section is assumed to be circular or is ignored altogether. The goal here is to develop an analytical/numerical model that overcomes some or all of these deficiences. In particular, it is desired to be able to predict gas jet behavior in supersonic crossflow by including enough of the important physical phenomena present so that the incorporation of empirical data becomes unnecessary. While the complexity of the problem requires introduction of a numerical procedure to predict the pressure and flowfield surrounding the jet, it is not our intention to produce a full-scale, three-dimensional numerical simulation. Rather, it is our hope that vortex models such as this will become useful in predicting fundamental transverse jet behavior for a variety of flow regimes, with a minimum in required computational time, so that parametric studies required for air breathing engine design can be completed easily and at low cost to the user.

## Vortex Modeling and the Outer Flow Solution

As mentioned above, the cross sections of gaseous jets in subsonic and supersonic crossflows tend to be kidney shaped or approximately elliptical in nature.[1, 6-8] We also note that a vortex pair structure has been observed to dominate the jet cross section in gas jets in low subsonic crossflows[6,7,12] and in supersonic crossflow.[1,8] Models that place emphasis on the dynamics of the vortex pair structure have been shown to successfully represent jets in incompressible and subsonic crossflows. Fearn and Weston[7] and LeGrives[13] have developed semianalytic vortex models for computing trajectories of gaseous jets in incompressible crossflows, whereas Karagozian[14] has developed a fully analytic model that holds under similar circumstances. This incompressible model is locally two-dimensional and assumes the jet cross section to be comprised of a counter-rotating viscous vortex pair. Viscous forces separating the vortices allow computation of the vortex pair half-spacing along the trajectory. The model also incorporates a mometum balance along the jet, as well as a representation for vortex strength, which accounts for jet impulse and viscous forces at the periphery of the jet cross section. The model accounts for mixing and predicts vortex separation and, thus, the variation in jet cross-sectional area along the entire trajectory.

Of course, such a model could not be used directly in a highly compressible supersonic stream, but the general approach does eliminate several of the deficiencies associated with previous models in this flow regime. The very recent work of Moore and Pullin[15] and Heister[16] suggests that a solution can be obtained for a compressible vortex pair that can serve as a basis for a compressible version of the Karagozian model. The presence of the bow shock presents serious problems for an analytical prediction of the pressure field surrounding the jet, and for this reason, a numerical approach after Godunov et al.[17] is constructed to solve the nonisentropic outer flowfield. Combination of this result with a compressible vortex solution provides the basis for the modeling efforts described herein.

Figure 1 presents a schematic description highlighting the primary elements contained in the present model. The description is similar to that of a recently developed gas jet model for subsonic crossflow,[18] with the exception of the bow shock, which envelopes the cross section of the jet. For the present, the wall boundary layer and its associated shock structures are neglected. In addition, shocks along the jet trajectory itself are neglected, which limits the applicability of the model to perfectly or sightly underexpanded jets.

As in the subsonic jet problem, the injection may be described in dimensionless form by considering six parameters: freestream and jet Mach numbers $M_\infty$ and $M_j$, respectively, jet-to-crossflow momentum flux ratio $R$, jet-to-crossflow velocity ratio $U_{jo}$, and specific heat ratios $\gamma$ and $\gamma_j$. All properties here are nondimensionalized in terms of freestream density, freestream velocity, and jet orifice diameter $d$.

The jet-to-crossflow momentum flux ratio, $R \equiv \rho_{jo}U_{jo}^2$, may also be expressed in terms of the initial jet-to-crossflow pressure ratio, $p_{jo}/p_\infty$:

$$R = (\gamma_j p_{jo} M_j^2)/(\gamma p_\infty M_\infty^2) \quad (1)$$

Again, the pressures here are made nondimensional by the freestream dynamic pressure. Hence, $\rho_{jo}$,$p_{jo}$, and $p_\infty$ are not initial inputs, but may be calculated in terms of input quantities:

$$\rho_{jo} = R/U_{jo}^2 \quad (2)$$

$$p_{jo} = R/(\gamma_j M_j^2) \text{ and } p_\infty = 1/(\gamma M_\infty^2) \quad (3)$$

Of course, according to the nondimensionalization employed, $\rho_\infty = U_\infty = 1$.

In order to calculate the force acting to separate the vortices associated with the jet cross section, the complete solution for the flowfield of a compressible vortex pair in crossflow is required. This solution is provided in detail in Ref. 16, and to a more limited extent, in Ref. 18. Figure 2 highlights some of the physical differences between compressible and incompressible vortex pair recirculation cells. The incompressible cell enjoys a symmetry about both $x$ and $y$ axes, with intercepts at $x_o = \pm\sqrt{3}h$, $y_o \simeq \pm 2.09h$. The compressible recirculation cell is complicated by the presence of vacuum cores that surround each vortex center, as well as the possibility of a shock existing in the recirculating region ($x > 0$) due to flow deceleration. The vacuum cores arise from the fact that there is a maximum achievable flow speed in a compressible fluid, at which vacuum conditions exist. Since for a compressible vortex one can show that $qr$ = constant, where $q$ is the flow speed and $r$ the radial distance from the vortex center, we must have a vacuum region surrounding the center of any compressible vortex. The vacuum core increases in size as the freestream Mach number increases. The numerical solution of Heister[16] for this problem relies on the assumption that, far from the vortex pair, the flowfield can be approximated as a vortex doublet with linearized (Prandtl-Glauert) compressibility effects. The fully two-dimensional potential equation is solved using the method of Osher et al.[19] in the region where nonzero density exists, and a special treatment is required within the vacuum core. The Osher scheme allows for the presence of weak shocks, since the entropy jump across the shock is third-order in the shock strength. Results of the calculations yield flow solutions for freestream Mach numbers up to $M_\infty = 0.3$. Above this limit, the vacuum core grows to be a dominant feature of the cell and errors associated with the vacuum core boundary condition preclude a numerical solution.

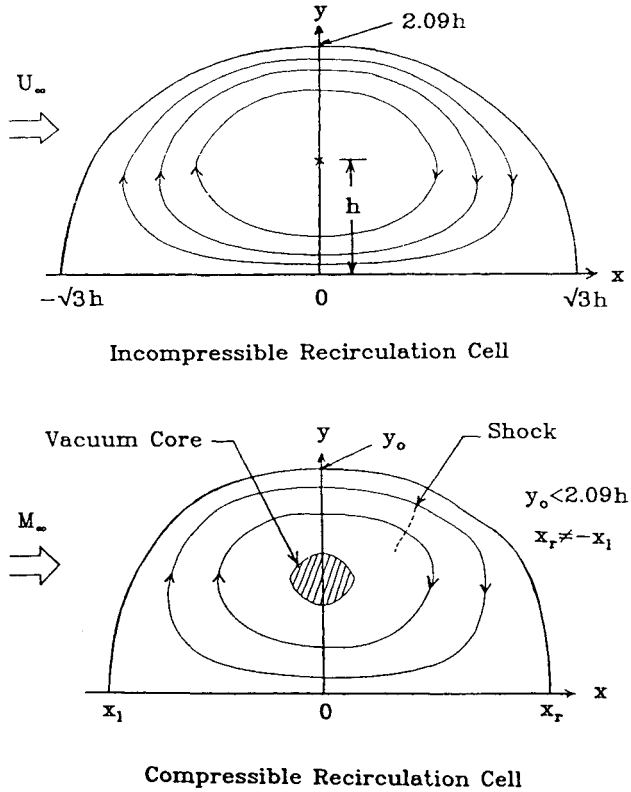


**Fig. 2 Comparison of the features of incompressible and compressible vortex pair recirculation cells.**

In order to resolve the flowfield and bow shock that can form about the (roughly elliptical) jet cross section, it becomes necessary to incorporate a fully numerical scheme to solve the two-dimensional Euler equations. The first-order method developed by Godunov et al.[17] has been found to be most appropriate to the present problem, in that: 1) the method is stable over a wide range of upstream Mach numbers, 2) the scheme is computationally more efficient than second-order schemes, 3) the technique performs well if no complex shock interactions are present, and 4) the scheme can be upgraded to second-order accuracy using TVD methods,[20] if required. A grid generation methodology that makes use of the elliptical nature of the vortex pair recirculation cell simplifies the calculations considerably. Details of this analysis and the numerical solution may be found in Ref. 21. Numerical resolution of the bow shock shape and flow characteristics is found to compare very well with experimental and other numerical solutions for compressible flows over ellipses and circles, where the upstream Mach number is greater than 0.5. Below this value, the Godunov scheme proves too inaccurate to obtain reasonable results, and a second-order scheme has to be introduced to resolve the flow at lower subsonic conditions. As will be shown, however, it becomes unnecessary to perform a second-order calculation for the present application to supersonic crossflows.

## Vortex Model for the Gas Jet in Supersonic Crossflow

The primary difficulty in the present modeling arises in characterizing the rotational, nonuniform flow behind the bow shock as an equivalent uniform upstream flow that can be used as input to the compressible vortex pair solutions described in Heister.[16] The model described in this section derives expressions for this equivalent flow in terms of freestream conditions, thus enabling a solution procedure much like that employed for the case of a subsonic crossflow[18] to be used. Making use of the Godunov solution for the external flow also will permit the calculation of wave drag on the cross section of the jet. This additional force must be taken into account in deriving an expression for the local jet orientation angle, to be described below.

### "Equivalent" Properties behind Bow Shock and External Flowfield Results

The flow situation seen by the transverse jet cross section is outlined schematically in Section A-A of Fig. 1. As $M_\infty \sin\phi_v$ increases, the upstream bow shock strength increases and the flow behind the shock becomes more stagnant relative to the freestream flow. The equivalent properties behind the bow shock that will characterize flow ahead of the jet cross section must take this fact into account. For a given cross-sectional geometry, the flowfield about the jet may be calculated using the Godunov scheme mentioned above, but the actual jet geometry is dependent on the equivalent Mach number of the compressed flow behind the shock, $M_{eq}$. For this reason, it is desirable to derive an expression for $M_{eq}$ that depends only on freestream conditions, so that the jet geometry can be characterized for all upstream conditions. Since the cross section as typically oriented is quite bluff, we approximate $M_{eq}$ as equal to the Mach number behind a normal shock occurring at the local freestream Mach number $M_\infty \sin\phi_v$. Of course, when $M_\infty$

$\sin\phi_v \leq 1$, no shock is present, and no transformation is required. Thus making use of standard normal shock relations, we write

$$M_{eq} = \left[\frac{(\gamma\text{-}1)(M_\infty \sin\phi_v)^2 + 2}{2\gamma(M_\infty \sin\phi_v)^2\text{-}(\gamma\text{-}1)}\right]^{1/2} \qquad (M_\infty \sin\phi_v > 1)$$

$$= M_\infty \sin\phi_v \qquad (M_\infty \sin\phi_v \leq 1) \tag{4}$$

From the equivalent Mach number obtained from Eq. (4), the jet cross section can be determined and numerical solutions of the outer flow may be performed. Results of these computations give detailed pressure and density distributions about the jet cross section, the wave drag, and the bow shock standoff distance for $0.8 < M_\infty \sin\phi_v < 5$. These results indicate that a shock forms near the rearward side of the jet cross-sectional slice at $M_\infty \sin\phi_v \cong 0.8$, so that wave drag is present for all $M_\infty \sin\phi_v$ above this value.

To increase the computational efficiency of this model, we can curve fit results of these calculations. The resulting drag coefficient for the jet cross section $C_D$, and bow shock standoff distance as measured from the center of the vortex pair $D_{bs}$ can be represented according to the following relations:

$$C_D = 1.2 + 0.543/(M_\infty \sin\phi_v)^2 \qquad (M_\infty \sin\phi_v \geq 1)$$

$$= -6.96 + 8.7 M_\infty \sin\phi_v \qquad (0.8 < M_\infty \sin\phi_v < 1)$$

$$= 0 \qquad (M_\infty \sin\phi_v < 0.8) \tag{5}$$

$$D_{bs} = 1.162 + 3.5/(M_\infty \sin\phi_v - 1) \qquad (M_\infty \sin\phi_v > 1.1) \tag{6}$$

Here we note that $C_D$ and $D_{bs}$ are nondimensionalized by vortex pair half-spacing $\bar{h}$, so that an additional factor of $h \equiv h/d$ must be included to place them in proper dimensionless form.

To complete the characterization of the equivalent uniform flow, we require $p_{eq}$ and $\rho_{eq}$, the equivalent pressure and density values behind the bow shock. It is easy to argue that $p_{eq}$ must be equal to the average pressure around the jet cross section, since in a truly subsonic inviscid flow the pressure distribution must be symmetric about the top of the jet cross section. Using a similar argument, the equivalent density is set equal to the average density around the jet periphery. These averaged quantities are calculated from the numerical solutions and are curve fit as a function of $M_\infty \sin\phi_v$:

$$p_{eq} = p_\infty[0.405 + 0.426(M_\infty \sin\phi_v)^2] \qquad (M_\infty \sin\phi_v \geq 1.5)$$

$$= p_\infty[0.861 + 0.217(M_\infty \sin\phi_v)^2] \qquad (0.8 < M_\infty \sin\phi_v < 1.5)$$

$$= p_\infty \qquad (M_\infty \sin\phi_v \leq 0.8) \tag{7}$$

$$\rho_{eq} = 0.651 + 0.805 \ell n(M_\infty \sin\phi_v) \qquad (M_\infty \sin\phi_v \geq 2)$$

$$= 0.964 + 0.0565(M_\infty \sin\phi_v)^2 \qquad (0.8 < M_\infty \sin\phi_v < 2)$$

$$= 1 \qquad (M_\infty \sin\phi_v \leq 0.8) \tag{8}$$

Finally, we note that the $\rho_{eq}$ and $p_{eq}$ values are insensitive to jet cross-sectional geometry, so that the $M_{eq}$ assumptions in Eq. (4) are justified for the purposes of defining the jet geometry. Given $\rho_{eq}$, $p_{eq}$, and $M_{eq}$, we then calculate the velocity of the equivalent uniform flow $U_{eq}$ from the definition of Mach number:

$$U_{eq} = M_{eq}\sqrt{\gamma p_{eq}/\rho_{eq}} \tag{9}$$

**Relation Governing Local Jet Orientation Angle $\phi_v$**

In the problem of the gas jet in subsonic crossflow,[18] we develop an algebraic relation between the local jet orientation angle $\phi_v$ and local vortex strength by considering components of vorticity generation that occur parallel and perpendicular to the jet axis at the orifice. The expression for the local circulation of each vortex, nondimensionalized by $d$ and freestream velocity, is modeled by

$$\Gamma = 2\sin\phi_v + \frac{\pi}{8h}[R + R/(\gamma_j M_j^2) - 1/(\gamma M_\infty^2)]\cos\phi_v \tag{10}$$

where the coefficient of $\sin\phi_v$ describes the dimensionless circulation arising from viscous forces as the crossflow is deflected about the jet orifice, and the coefficient of $\cos\phi_v$ represents vorticity generation by the impulse associated with the jet. It is possible to define such a relation because the jet exhausts into a uniform flow with constant properties $\rho_\infty$ and $p_\infty$. In the case where the crossflow is supersonic, the jet exhausts into a flow which is locally nonuniform, since the shock strength varies with local jet orientation angle. In addition, wave drag is present and also contributes to jet deflection. The proper relation for $\phi_v$ must take both of these phenomena into account.

We first consider the relation between the orientation angle $\phi_v$ and the local dimensionless vortex circulation $\Gamma$. We incorporate the effective back pressure notion of Schetz et al.[9] and assume that the effective pressure experienced by the jet is simply the equivalent average pressure calculated by the inviscid outer flow solution, as in Eq. (7). Similarly, the density of the freestream gas corresponds to $\rho_{eq}$ [Eq. (8)]. Under these assumptions, the dimensionless circulation $\Gamma$ of each vortex may be expressed

$$\Gamma = 4\pi U_{eq} h = 2U_{eq} + \lambda\cos\phi_v/h \tag{11}$$

where

$$\lambda = (R + p_{jo} - p_{eqo})\pi/(8U_{eqo}\rho_{eqo})$$

$$= \text{constant} \tag{12}$$

The subscripts $(\,)_{jo}$ and $(\,)_{eqo}$ refer to orifice conditions in the jet and initial equivalent properties in the outer flow, respectively, and the term $(R + p_{jo} - p_{eqo})$ represents the thrust per unit area in the jet. The initial (orifice) condition for dimensionless vortex half spacing, $h_o = 1/2\pi$, applies as in the subsonic jet case and is evidenced by Eq. (11) when $\cos\phi_v = 0$. This condition results from equating the jet cross-sectional area at the orifice to the equivalent area of the vortex pair recirculation cell. Finally, we note that if the flow satisfies the condition $M_\infty \sin\phi_v < 0.8$, then $U_{eq} = \sin\phi_v$, $\rho_{eq} = \rho_\infty$, $p_{eq} = p_\infty$, and Eq. (10) can be recovered from Eqs. (11) and (12).

Now, in order to determine changes in $\phi_v$ due to changes in the local vortex circulation along the jet trajectory, we solve Eq. (11) for $\cos\phi_v$ and differentiate with respect to "flow" time $t$ to obtain

$$\lambda \sin\phi_v \frac{d\phi_v}{dt} + U_{eq}(8\pi h - 2)\frac{dh}{dt} + h(4\pi h - 2)\frac{dU_{eq}}{dt} = 0 \tag{13}$$

Using the definition of $U_{eq}$ in Eq. (9), we can write

$$\frac{dU_{eq}}{dt} = U_{eq}\left[\frac{dM_{eq}/dt}{M_{eq}} + \frac{dp_{eq}/dt}{2p_{eq}} - \frac{d\rho_{eq}/dt}{2\rho_{eq}}\right] \tag{14}$$

Now the expressions in Eqs. (4), (7), and (8) can be differentiated to give the required derivatives on the right side of Eq. (14). One can note that a factor of $d\phi_v/dt$ will be present in all

these derivatives, so that it is useful to define

$$\tilde{M}'_{eq} \equiv \frac{dM_{eq}/dt}{M_{eq}\,d\phi_v/dt}$$

with analagous definitions for $\tilde{p}'_{eq}$ and $\tilde{\rho}'_{eq}$. Using these definitions, Eq. (14) reduces to the form

$$\frac{dU_{eq}}{dt} = U_{eq}\frac{d\phi_v}{dt}\left[\tilde{M}'_{eq} + \frac{1}{2}(\tilde{p}'_{eq} - \tilde{\rho}'_{eq})\right] \tag{15}$$

Finally, substituting Eq. (15) into Eq. (13) gives changes in $\phi_v$ due to the local variation in vortex strength along the jet trajectory:

$$\left(\frac{d\phi_v}{dt}\right)_{circ} = \frac{-U_{eq}(8\pi h - 2)dh/dt}{\lambda \sin\phi_v + hU_{eq}(4\pi h - 2)(\tilde{M}'_{eq} + \frac{1}{2}(\tilde{p}'_{eq} - \rho'_{eq}))} \tag{16}$$

If no wave drag were present, Eq. (16) could be integrated to describe the behavior of $\phi_v$ as a function of flow time (or distance along the jet trajectory). However, with a supersonic crossflow, wave drag affects the jet cross section and, hence, it affects the calculation of the orientation angle $\phi_v$, even in the absence of a vortex pair structure. We can derive an expression for $d\phi_v/dt$ due to drag forces by balancing this force with the centripetal force on the jet cross section, as done, for example, in models of the transverse liquid jet[21, 22]:

$$-hC_D \sin^2\phi_v = \rho_j Bh^2 U_j^2 d\phi_v/ds \tag{17}$$

where $Bh^2$ is the dimensionless jet cross-sectional area, with $B = \pi^3/2$. The dimensionless distance $s$ is the coordinate measured along the jet and can be related to dimensionless flow time $t$ through $U_j$:

$$U_j = ds/dt \tag{18}$$

Combining Eqs. (17) and (18) produces a relation for changes in $\phi_v$ due to wave drag on the cross section of the jet:

$$\left(\frac{d\phi_v}{dt}\right)_{drag} = -C_D \sin^2\phi_v/(\rho_v U_j Bh) \tag{19}$$

The total change in $\phi_v$ is simply the sum of variations in $\phi_v$ due to circulation and due to wave drag effects:

$$\frac{d\phi_v}{dt} = \left(\frac{d\phi_v}{dt}\right)_{circ} + \left(\frac{d\phi_v}{dt}\right)_{drag} \tag{20}$$

Below $M_\infty \sin\phi_v = 0.8$, the wave drag term in Eq. (20) vanishes, and integration of Eq. (16) gives results equivalent to the algebraic expression employed in the case of a subsonic crossflow.[18]

### Force Balance in Jet Cross Section

The derivation of the force balance that provides the initial conditions and governing equation for the dimensionless vortex pair half-spacing $h$ evolves from calculation of the net compressible forces acting to separate the inviscid compressible vortices. These forces arise from 1) integration of the net pressure force acting on a closed streamline associated with each compressible vortex, and 2) the additional forces separating the vortices if the jet is underexpanded.

The first force term $F_y$ arises from the vacuum core surrounding each vortex and the shocks that may be present in the recirculating region. A curve fit of the relation between this force and upstream (equivalent) Mach number is

$$F_y = 3.02\, M_{eq}^{0.7} h \rho_{eq} U_{eq}^2 (p_j/p_c) \tag{21}$$

where $p_j$ is the local (current) jet pressure and $p_c$ is the (newly computed) average recirculation cell pressure. Clearly, as the freestream (or equivalent) Mach number approaches zero, so does $F_y$, which is consistent with the incompressible inviscid vortex pair flowfield. In this limit of the transverse jet problem, viscous forces tend to dominate the vortex separation process, as indicated by Karagozian.[14]

The second-force term in the present problem, $F_{yp}$, can be expressed in terms of the difference between the local jet pressure and the equivalent upstream pressure:

$$F_{yp} = \left(\frac{x_o}{y_o}\right)(p_j - p_{eq})h \tag{22}$$

where, for the entire Mach number range under consideration, the compressible solution of Heister[16] indicates that $x_o/y_o \cong 1.66$. Although this treatment is approximate, we are only considering slightly underexpanded jets, so that a pressure equilibrium is reached within 2-3 jet diameters of the orifice.

Application of Newton's second law to each vortex yields the following equation describing vortex pair half-spacing $h$:

$$\frac{d^2h}{dt^2} = \frac{F_y + F_{yp}}{w_j} - \left(\frac{1}{\rho_j}\frac{d\rho_j}{dt} + \frac{2}{h}\frac{dh}{dt}\right)\frac{dh}{dt} \tag{23}$$

and the following expression for the initial (orifice) condition for the rate of vortex separation:

$$(dh/dt)_{t=t_o} = h_o[2w_{jo}h_o/(F_{yo} + F_{ypo})]^{-1/2} \tag{24}$$

Here, $w_j = Bh^2\rho_j$ represents the dimensionless mass per unit length in the upper half of the recirculation cell.

### Mass and Momentum Balances along the Jet

As in the problem of the subsonic gas jet,[18] we allow no entrainment to take place until the jet is expanded to the local pressure $p_{eq}$ of the external flow. Beyond this point, the fluid is entrained at velocity $U_{eq}\cot\phi_v$ rather than $U_\infty \cos\phi_v$ as in the subsonic gas jet. Introducing these minor modifications, the mass balance performed along the jet trajectory becomes

$$\frac{d\rho_j}{dt} = -2\frac{\rho_j}{h}\frac{dh}{dt} \quad p_j > p_{eq}$$

$$= -2\frac{p_j}{h}\frac{dh}{dt} + k\rho_{eq}U_{eq}\cot\phi_v \quad p_j = p_{eq} \tag{25}$$

where $k$ represents the ratio of vortex pair recirculation cell perimeter to cell area and can be curve fit from numerical results to take the form

$$k = \left[1.024 + 1.4(M_{eq})^2\right]/h \tag{26}$$

The momentum balance along the trajectory accounts for mass addition and pressure variation and reduces to the form

$$\frac{dU_j}{dt} = \frac{\left[\frac{1}{\rho_j}\frac{d\rho_j}{dt}\left(U_{eq}\cot\phi_v - U_j - \frac{\gamma_j p_j}{\rho_j U_j}\right) + (U_{eq}\cot\phi_v - U_j)\frac{2}{h}\frac{dh}{dt}\right]}{\left(2 - \frac{U_{eq}\cot\phi_v}{U_j}\right)} \tag{27}$$

This yields a relation for variation of jet velocity $U_j$ in terms of $\rho_j$ and derivatives of $h$ only.

**Bow Shock and Jet Centerline Coordinates**

The jet centerline coordinates $(X,Z)$ are obtained, as in the subsonic gas jet, by integrating the solution for $U_j$ [from Eq. (25)] according to the relations

$$X = \int_{t_o}^{t} U_j \cos\phi_v dt \tag{28a}$$

$$Z = \int_{t_o}^{t} U_j \sin\phi_v dt \tag{28b}$$

The bow shock coordinates $(X_s, Z_s)$ can then be calculated from $(X, Z)$, using the shock standoff distance $D_{bs}$:

$$X_s = X - D_{bs}\, h \sin\phi_v \tag{29a}$$

$$Z_s = Z - D_{bs}\, h \cos\phi_v \tag{29b}$$

The $h$ value in Eqs. (29) is allowed to grow to the point where the jet is perfectly expanded and is then held fixed for the remainder of the trajectory. This approach is reasonable, since growth in $h$ beyond this point is a result of the entrainment of freestream fluid, which does not effectively increase the obstruction leading to the ultimate shock standoff distance.

The four ordinary differential equations [Eqs. (20), (23), (25), and (27)] are now integrated numerically using Huen's method with a dimensionless step size of 0.025. The code is about 200 lines and runs in only a few seconds on an IBM 3090 computer. Typical runs contain 800–1000 points along the jet trajectory.

## Results and Discussion

Descriptions of the model results are presented here, with comparisons made with experimental data so as to validate the model. Although many experiments have been performed (see Introduction), the bulk of these tests have focused on thrust vector control applications and have given little data regarding the actual trajectory of the jet. In addition, most researchers employ highly underexpanded jets, which have strong Mach disk shocks that cannot be resolved using the current model. Orth et al.[23] present some trajectory data for perfectly and slightly underexpanded jets in the $M_\infty = 2$–3 range using hydrogen and air injection. The recent experiments of McDaniel and Graves[8] do consider the case of the slightly underexpanded gas jet in supersonic crossflow ($M_\infty = 2.07$), although the jets are injected into a confined duct in which the opposite wall and external shock reflections influence the jet and its own shock structure. In addition, these experiments measure

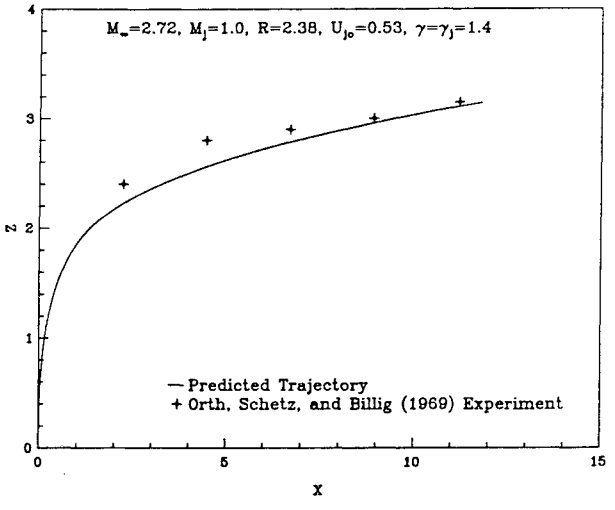


Fig. 3a Comparison of computed jet trajectories with the experimental results of Orth et al.[23]

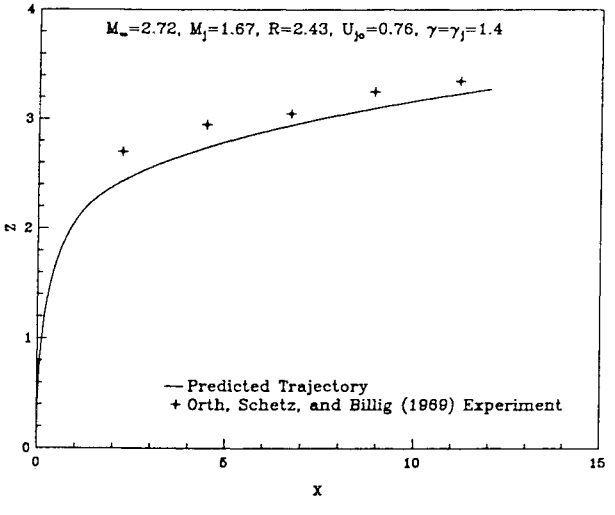


Fig. 3b Comparison of computed jet trajectories with the experimental results of Orth et al.[23]

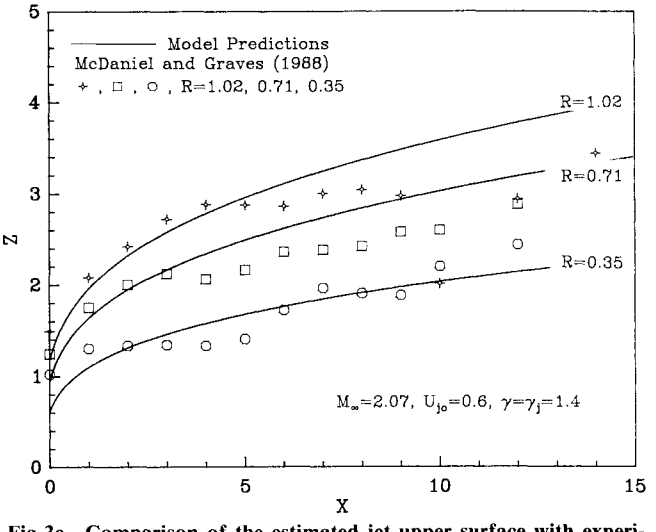


Fig.3c Comparison of the estimated jet upper surface with experimental results of McDaniel and Graves.[8]

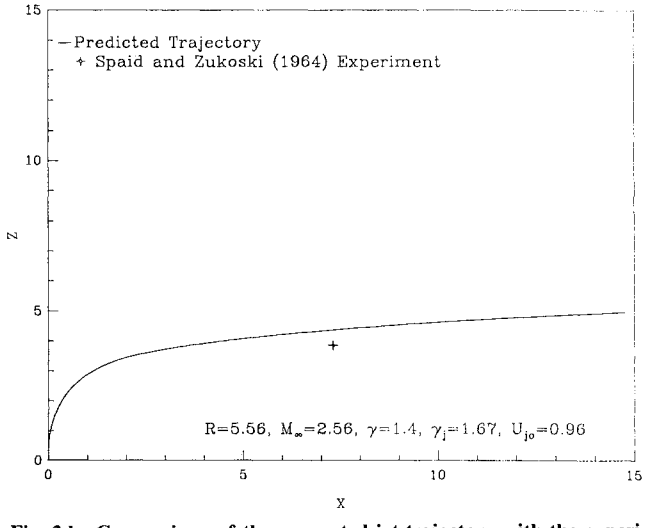


Fig. 3d Comparison of the computed jet trajectory with the experimental results for sonic jet penetration of Zukoski and Spaid.[1]

the visible top of the jet rather then the centerline of the trajectory, which is more closely predicted by the present model.

Figures 3a and 3b present comparisons of the model with the experimental data of Orth et al.[23] for $M_j = 1$ and 1.67, respectively. The experimental points represent the locus of maximum $H_2$ concentration, although the model prediction is actually for the center of mass within the vortex pair recirculation cell. Both curves show good agreement (within 10%) over the entire jet curve, although the experimental points tend to lie above the predicted trajectory. This inconsistency is easily explained, since the concentration profiles measured in Orth et al.[23] are biased toward $Z = 0$, so that the center of mass lies below the point of maximum concentration.

Comparisons of model predictions with experimental data for the top of a gas jet in $M_\infty = 2.07$ crossflow are shown in Fig. 3c, for several different momentum ratios. In order to estimate the spread of the jet for this particular configuration, the dimensionless distance from the center of the ellipse to the $x$-intercept, $x_\ell$, is computed using the compressible vortex pair solution of Heister.[16] This dimensionless distance can be approximated as

$$x_\ell \cong \sqrt{3}\left[1 - (1.2)M_{eq}^2\right]h \tag{30}$$

which reduces to the appropriate expression when $M_{eq} \to 0$. The overall comparison of the model predictions with the data is good (within 15%), despite the fact that the experimental data are influenced by the duct height, especially at high momentum flux ratios, and that reflection shocks cause significant waviness in the data.

One final comparison is shown in Fig. 3d, where the predicted jet trajectory is compared with the jet penetration depth observed by Zukoski and Spaid.[1] Although this experiment actually examines a highly underexpanded jet ($p_{jo}/p_{eqo} \cong 10$), the prediction by the model is still quite reasonable. The present model should be considered most appropriate, however, in the range $1 \le p_{jo}/p_{eqo} \le 4$.

We next turn to investigate the various parameters governing the injection process. Variation of the gas ratio of specific heats has no appreciable effect of jet trajectories, so this parameter is eliminated from the investigation. We should point out that this conclusion is verified by experiments of Chrans and Collins, [24] who found no influence of molecular weight (and, hence, specific heat) on jet trajectory. The most influential parameter in determining jet penetration is the momentum flux ratio $R$, as is demonstrated in Fig. 4. In this figure, $R$ is varied from 0.47 to 1.41 at a fixed jet injection density of unity and for a freestream Mach number of 3. These three momentum flux ratios correspond to $p_{jo}/p_{eqo} < 1$,

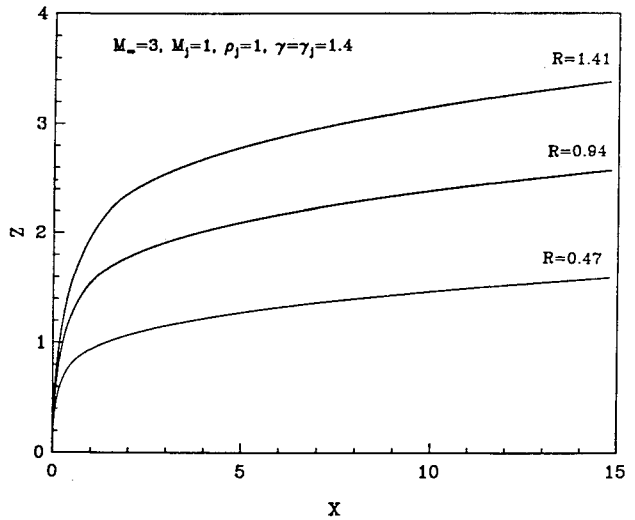


Fig. 4 Effect of momentum ratio $R$ on jet trajectory.

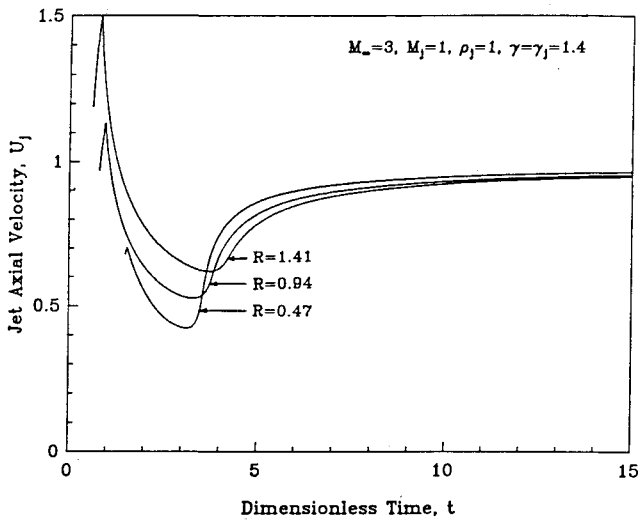


Fig. 5 Jet axial velocity histories for $M_\infty = 3$.

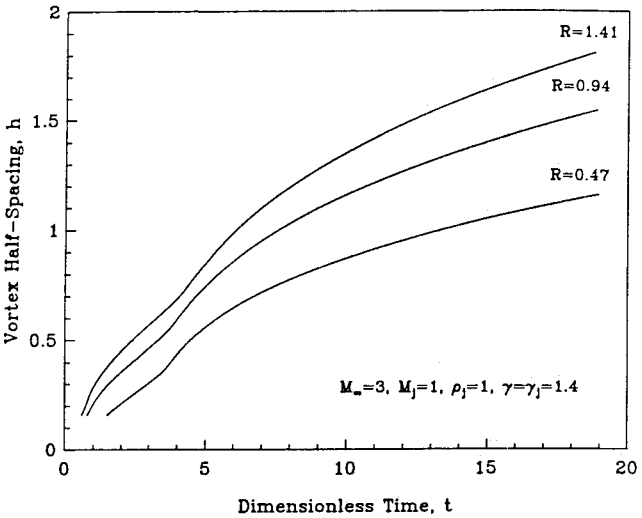


Fig. 6 Vortex spacing histories for $M_\infty = 0.3$.

2, 3, respectively. The results indicate that the jet penetration scales nearly linearly with $R$, since a tripling of $R$ nearly triples the overall penetration of the jet.

Figure 5 presents jet axial velocity as a function of flow time for the three curves in Fig. 4. The nearly perfectly expanded jet ($R = 0.47$) shows an immediate decrease in $U_j$, followed by an asymptotic increase to the freestream velocity. Jet velocity increases rapidly for a short period of time in the underexpanded jets ($R = 0.94$, 1.41) but drops rapidly due to entrainment of outer fluid and retains the same asymptotic behavior as the perfectly expanded jet. Figure 6 shows the vortex spacing histories for the jets of Fig. 4. A sharp increase in $h$ in the transonic region ($M_\infty \sin\phi_v \cong 1$) causes the inflections present in each of the three curves. The asymptotic behavior is similar to the subsonic gas jets[18] and the incompressible jet results given by Karagozian. [14]

Further investigation reveals that $F_y$, the force tending to separate the vortices, is the cause of the inflections in the vortex spacing curves of Fig. 6. Figure 7 presents $F_y$ as a function of $M_\infty \sin\phi_v$ for the parameters used in the center curve of Fig. 6. This figure demonstrates a sharp increase in $F_y$ in the transonic range, with the peak value at $M_\infty \sin\phi_v = 1$. At higher $M_\infty \sin\phi_v$ values, the presence of the bow shock tends to produce a more benign environment in terms of the equivalent Mach number characterizing the vortex pair. At high $M_\infty \sin\phi_v$, the jet is "shielded" by the bow shock and wave drag provides the dominate contribution to the dynamics of the jet.

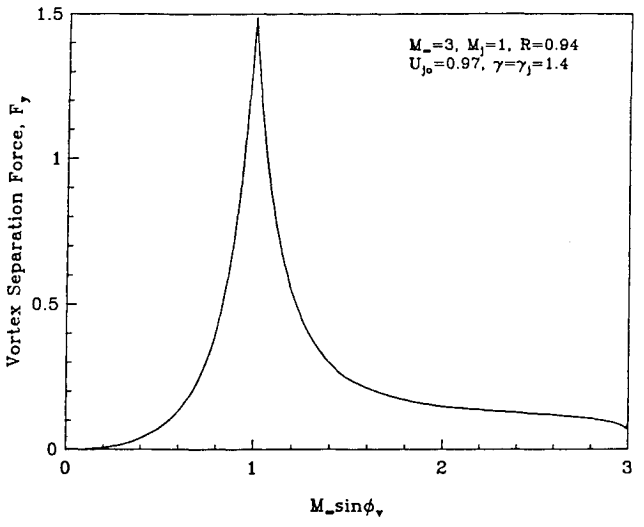


Fig. 7 Influence of Mach number normal to the jet cross section ($M_\infty \sin\phi_v$) on the force tending to separate the vortices ($F_y$).

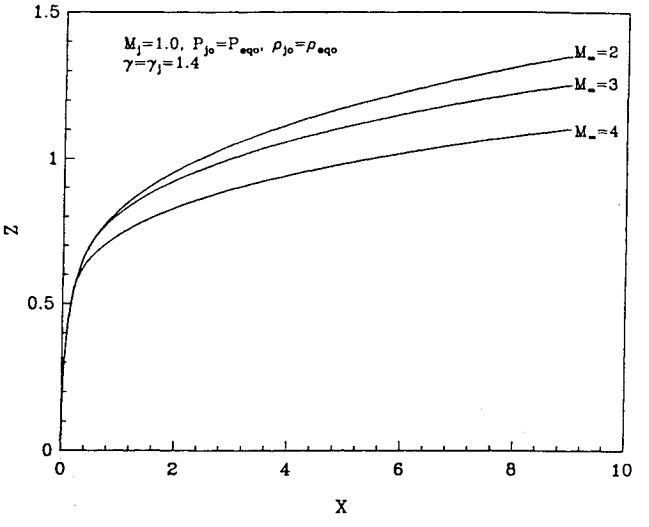


Fig. 8b Effects of $M_\infty$ on perfectly expanded ($p_{jo} = p_{eqo}$) sonic jets.

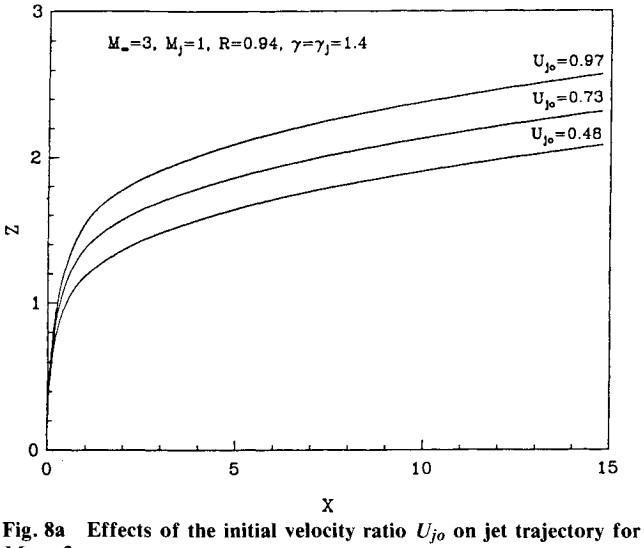


Fig. 8a Effects of the initial velocity ratio $U_{jo}$ on jet trajectory for $M_\infty = 3$.

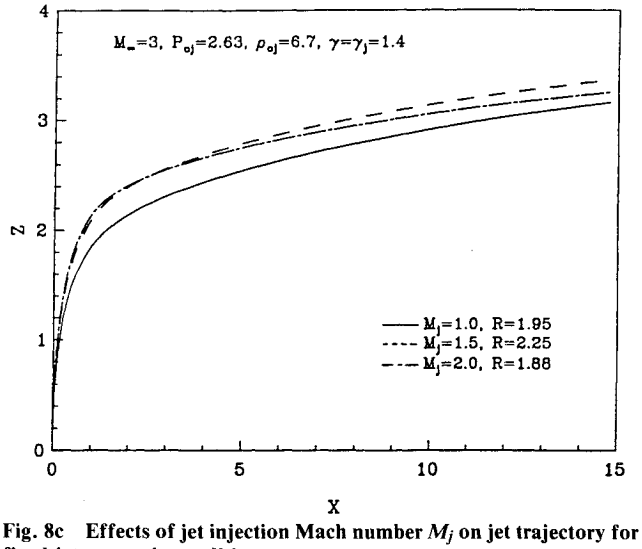


Fig. 8c Effects of jet injection Mach number $M_j$ on jet trajectory for fixed jet reservoir conditions.

The effects of initial velocity ratio are demonstrated for a sonic jet at $M_\infty = 3$, $R = 0.94$ in Fig. 8a. Increasing $U_{jo}$ appears to have a greater influence in the the supersonic crossflow as compared to the subsonic crossflow (see Ref. 18). In the subsonic case, doubling $U_{jo}$ increases penetration by 12%, whereas Fig. 8a demonstrates a 24% increase in penetration by doubling $U_{jo}$.

Figure 8b demonstrates the effects of $M_\infty$ on "perfectly expanded" ($p_{jo} = p_{eqo}$) sonic jets. This figure demonstrates the need for jet underexpansion to maximize penetration, since these perfectly expanded jets realize an overall penetration of only 1-2 orifice diameters. The influence of $M_\infty$ is primarily due to drag increases, since jet momentum increases with $M_\infty$ in order to keep $p_{jo} = p_{eqo}$.

The final parameter we investigate is the jet injection station Mach number. One can assess the effects of this parameter as well as orifice design by looking at a jet with fixed reservoir stagnation conditions. Figure 8c demonstrates the effects of varying $M_j$ from 1 to 2 under these conditions the $M_j = 2$ jet is perfectly expanded and $p_{jo}/p_{eqo} = 2.1$, 4.1 for $M_j = 1.5$, 1 respectively. The trajectories of Fig. 12 demonstrate that an optimum $M_j$ exists that will maximize penetration. Although the $M_j = 1.5$ and $M_j = 1$ curves are very close to each other, the $M_j = 1$ jet will realize higher shock losses because it is more highly underexpanded. The optimum $M_j$ appears to be somewhere below $M_j = 2$, which implies orifice expansion ratios less than 1.7. It would be desirable to incorporate a Mach disk model into the code so that this optimization could be performed more accurately.

The present vortex model for a gaseous jet in supersonic crossflow represents the first attempt ever (to our knowledge) to predict jet trajectories without the aid of empirical correlations. The model is currently limited to freestream Mach numbers below 5, due to limitations in the external flow (Godunov) solution, but could easily be extended to higher $M_\infty$ if dissociation of the outer flow is taken into account. This model serves as an excellent design tool, as it is able to predict overall penetration to within 10-15% while using only a few seconds of computer time. The model is, however, most appropriate for perfectly or slightly expanded jets; a Mach disk model would be required to study and predict the behavior of highly underexpanded jets. These and other complexities associated with this flowfield will be explored in future modeling efforts.

## References

[1]Zukoski, E.E., and Spaid, F.W., "Secondary Injection of Gases into a Supersonic Flow," *AIAA Journal*, Vol. 2, Oct. 1964, pp. 1689-1696.

[2]Spaid, F.W., and Zukoski, E.E., "Further Experiments Concerning Secondary Injection of Gases into a Supersonic Flow," *AIAA Journal*, Vol. 4, Dec. 1966, pp. 2216-2218.

[3]Broadwell, J.E., "Analysis of the Fluid Mechanics of Secondary Jet Injection for Thrust Vector Control," *AIAA Journal*, Vol. 1, May 1963, pp. 1067-1075.

[4]Charwat, A.F., and Allegre, J., "Interaction of a Supersonic Stream and a Transverse Supersonic Jet," *AIAA Journal*, Vol. 2, Nov. 1964, pp. 1965-1972.

[5]Hsia, H.T., Seifert, H.S., and Karamcheti, K., "Shocks Induced by Secondary Fluid Injection," *Journal of Spacecraft*, Vol. 2, Jan. 1965, pp. 67-72.

[6]Kamotani, Y., and Greber, I., "Experiments on a Turbulent Jet in a Crossflow" *AIAA Journal,* Vol. 10, Nov. 1972, pp. 1425-1429.

[7]Fearn, R., and Weston, R.P., "Vorticity Associated with a Jet in a Cross Flow," *AIAA Journal,* Vol. 12, Dec. 1974, pp. 1666-1671.

[8]McDaniel, J.C., and Graves, J., "Laser-Induced Fluorescence Visualization of Transverse Gaseous Injection in a Nonreacting Supersonic Combustor," *Journal of Propulsion and Power,* Vol. 4, Nov.-Dec. 1988, pp. 591-597.

[9]Schetz, J.A., Hawkins, P.F., and Lehman, H., "Structure of Highly Underexpended Transverse Jets in a Supersonic Stream," *AIAA Journal,* Vol. 5, May 1967, pp. 882-884.

[10]Schetz, J.A., and Billig, F.S., "Penetration of Gaseous Jets Injected into a Supersonic Stream," *Journal of Spacecraft,* Vol. 3, Nov. 1966, pp. 1658-1665.

[11]Billig, F.S., Orth, R.C., and Lasky, M., "A Unified Analysis of Gaseous Jet Penetration," *AIAA Journal,* Vol. 9, June 1971, pp. 1048-1058.

[12]Abramovich, G.N., *Theory of Turbulent Jets,* MIT Press, Cambridge, MA, 1963.

[13]LeGrives, E., "Mixing Process Induced by the Vorticity Associated with the Penetration of a Jet into a Crossflow," *Journal of Engineering for Power,* Vol. 100, 1978, pp. 465-475.

[14]Karagozian, A.R., "An Analytical Model for the Vorticity Associated with a Transverse Jet," *AIAA Journal*, Vol. 24, March 1986, pp. 429-436.

[15]Moore, D.W., and Pullin, D.I., "The Compressible Vortex Pair," *Journal of Fluid Mechanics,* Vol. 195, 1987, pp. 171-204.

[16]Heister, S.D., "Transverse Jets in Compressible Crossflows," Ph.D. Dissertation, Univ. of California, Los Angeles, CA, 1988.

[17]Godunov, S.K., Zabrodin, A.V., and Prokopov, G.P., "A Computational Scheme for Two-Dimensional Non-Stationary Problems of Gas Dynamics and Calculation of the Flow from a Shock Wave Approaching a Steady State," *U.S.S.R. Computational Mathematics and Math Physics,* 1961, pp. 1187-1219.

[18]Heister, S.D., and Karagozian, A.R., "Vortex Modeling of Gaseous Jets in Compressible Crossflow," *Journal of Propulsion and Power*, Vol. 6, Jan.-Feb. 1990, pp. 85-92.

[19]Osher, S., Whitlow, W., and Hafez, M., "Entropy Condition Satisfying Approximations for the Full Potential Equations of Transonic Fluid Flow," NASA TM 85751, Jan. 1984.

[20]Harten, A., "High Resolution Schemes for Hyperbolic Conservation Laws," *Journal of Computational Physics,* Vol. 49, 1983, pp. 357-393.

[21]Heister, S.D., Nguyen, T.T., and Karagozian, A.R., "Modeling of Liquid Jets Injected Transversely into a Supersonic Crossflow," *AIAA Journal*, Vol. 27, Dec. 1989, pp. 1727-1734.

[22]Catton, I., Hill, D.E., and McRae, R.P., "Study of Liquid Jet Penetration in a Hypersonic Stream," *AIAA Journal,* Vol. 6, Nov. 1968, pp. 2084-2089.

[23]Orth, R.C., Schetz, J.A., and Billig, F.S., "The Interaction and Penetration of Gaseous Jets in Supersonic Flow," NASA CR-1386, July 1969.

[24]Chrans, L.J., and Collins, D.J., "Stagnation Temperature and Molecular Weight Effects in Jet Penetrations," *AIAA Journal,* Vol. 8, Feb. 1970, pp. 287-293.

*Recommended Reading from the AIAA Progress in Astronautics and Aeronautics Series . . .* AIAA

**Numerical Methods for Engine-Airframe Integration**

*S. N. B. Murthy and Gerald C. Paynter, editors*

Constitutes a definitive statement on the current status and foreseeable possibilities in computational fluid dynamics (CFD) as a tool for investigating engine-airframe integration problems. Coverage includes availability of computers, status of turbulence modeling, numerical methods for complex flows, and applicability of different levels and types of codes to specific flow interaction of interest in integration. The authors assess and advance the physical-mathematical basis, structure, and applicability of codes, thereby demonstrating the significance of CFD in the context of aircraft integration. Particular attention has been paid to problem formulations, computer hardware, numerical methods including grid generation, and turbulence modeling for complex flows. Examples of flight vehicles include turboprops, military jets, civil fanjets, and airbreathing missiles.

***TO ORDER:*** **Write, Phone, or FAX:** AIAA c/o TASCO, 9 Jay Gould Ct., P.O. Box 753, Waldorf, MD 20604 Phone (301) 645-5643, Dept. 415 ■ FAX (301) 843-0159

Sales Tax: CA residents, 7%; DC, 6%. For shipping and handling add $4.75 for 1-4 books (call for rates for higher quanties). Orders under $50.00 must be prepaid. Foreign orders must be prepaid. Please allow 4 weeks for delivery. Prices are subject to change without notice. Returns will be accepted within 15 days.

**1986 544 pp., illus. Hardback**
**ISBN 0-930403-09-6**
**AIAA Members $54.95**
**Nonmembers $72.95**
**Order Number V-102**